SUPPORTING INFORMATION

CO and O_2 Binding to Pseudo-Tetradentate Ligand-Copper(I)-Complexes with a Variable N-Donor Moiety: Kinetic/Thermodynamic Investigation Reveals Ligand Induced Changes in Reaction Mechanism

Heather R. Lucas, Gerald J. Meyer, and Kenneth D. Karlin**

Department of Chemistry, The Johns Hopkins University, Baltimore, Maryland 21218

TABLE OF CONTENTS:

Figure S13. Temperature dependence and [CO] dependence of pseudo-first order CO recombination to $^{Bz}\mathbf{Cu^{I}}$ in THF (k_{obs} vs. [CO]), 213 – 293 K. The slope of each line corresponds directly to the bimolecular rate constant of CO recombination, k_{CO} (M^{-1} s^{-1}).

Figure S14. Eyring analysis of bimolecular CO recombination to $^{Bz}\mathbf{Cu^{I}}$ in THF solvent at various temperatures, 213 – 293 K.

Figure S15. UV-visible spectra in MeTHF at −128 °C illustrating the formation of the dicopper(II)-μ-1,2-peroxo of BPQA $\mathbf{[\{^{Q}LCu^{II}\}_2(O_2^{2-})]^{2+}}$ following the addition of O_2 to $^{Q}\mathbf{LCu^{I}}$.

Figure S16. Transient absorption difference spectra illustrating the slow equilibration (k_{slow}) from $^{Im}\mathbf{LCu^{II}\text{-}O_2^{-}}$ to $^{Im}\mathbf{LCu^{I}\text{-}CO}$ in THF at −80 °C at various delay times.

Table S2. Bimolecular rate constants k_{O2} determined from k_{slow} for $^{Im}\mathbf{LCu^{II}\text{-}O_2^{-}}$ and $^{NMe_2}\mathbf{LCu^{II}\text{-}O_2^{-}}$ at various temperatures.

Figure S17. Plot of $1/k_{slow}$ vs. $[O_2]/[CO]$ at –67 °C for determination of K_{O2} and k_{-O2} for $^{Im}\mathbf{LCu^{II}\text{-}O_2^{-}}$, which readily gives to k_{O2}.

Figure S18. Eyring analysis plot for formation of $^{Im}\mathbf{LCu^{II}\text{-}O_2^{-}}$ of the k_{O2} data collected at variable temperature (–85 °C to –60 °C).

Figure S19. Eyring analysis plot for formation of $^{Im}\mathbf{LCu^{II}\text{-}O_2^{-}}$ of the k_{-O2} data collected at variable temperature (–85 °C to –60 °C).

Figure S20. Van't Hoff plot of variable temperature K_{O2} data for $^{Im}\mathbf{LCu^{II}\text{-}O_2^{-}}$ collected from –85 °C to –60 °C.

Figure S21. Plot of $1/k_{slow}$ vs. $[O_2]/[CO]$ at –65 °C for determination of K_{O2} and k_{-O2} for $^{NMe_2}\mathbf{LCu^{II}\text{-}O_2^{-}}$, which readily gives to k_{O2}.

Figure S22. Eyring analysis plot for formation of $^{NMe_2}\mathbf{LCu^{II}\text{-}O_2^{-}}$ of the k_{O2} data collected at variable temperature (–85 °C to –60 °C).

Figure S23. Eyring analysis plot for formation of $^{NMe_2}\mathbf{LCu^{II}\text{-}O_2^{-}}$ of the k_{-O2} data collected at variable temperature (–85 °C to –60 °C).

Figure S24. Van't Hoff plot of variable temperature K_{O2} data for $^{NMe_2}\mathbf{LCu^{II}\text{-}O_2^{-}}$ collected from –85 °C to –60 °C.

EXPERIMENTAL.

Materials and Methods. All reagents were purchased from commercial sources. All air sensitive compounds were synthesized utilizing standard Schlenk techniques. Elemental analyses were performed by Desert Analytics (Tucson, AZ) or Quantitative Technologies, Inc. (QTI, Whitehouse, NJ). ^{1}H NMR spectra were recorded at 400 MHz on a Bruker Avance FT-NMR spectrometer. Chemical shifts were reported as δ values relative to an internal standard (Me_4Si) and the residual solvent proton peak. Deuterated nitromethane (CD_3NO_2) was purchased from Aldrich (99%) and deaerated under nitrogen gas (N_2; Air Gas East, grade 4.8). Diethyl ether (Et_2O; Fisher Scientific 99+%) and tetrahydrofuran (THF; EMD 99%) solvents were purified by passing through a series of activated alumina columns (Innovative Technology, Newburyport, MA) under nitrogen gas. Under an argon (Air Gas East, grade 4.8) atmosphere, the solvents were further dried through distillation over calcium hydride for Et_2O and elemental sodium for THF. Pentane (Fisher Scientific 99%) and acetonitrile (CH_3CN; Fisher Scientific 99.9%) solvent were dried and distilled over calcium hydride, while 2-methyl-tetrahydrofuran (Me-THF; Sigma-Aldrich ≥99%) was distilled over small pieces of sodium. The dry solvents (Et_2O, THF, pentane, CH_3CN) were then sparged with argon gas for one hour and introduced under vacuum to an MBraun Labmaster 130 dry box (O_2 < 1 ppm; H_2O < 1 ppm). The dry and deoxygenated solvents were stored within the drybox in amber bottles containing a thin layer of activated molecular sieves (4 Å).

Synthesis.

^{Q}LCu^{I}. In a 50 mL Schlenk flask equipped with a stirbar, a 10 – 15 mL deoxygenated Et_2O solution of BPQA (46 mg, 0.16 mmol) was added to one equivalent of $[Cu^{I}(MeCN)_4]B(C_6F_5)_4$ (144 mg, 0.16 mmol) under an argon atmosphere. The solution was stirred under an argon environment for 20 minutes. Deoxygenated pentane (50 ml) was then added to the bright yellow solution

resulting in the precipitation of a yellow solid. The solution was removed through a cannula and the solid was dried under vacuum. The solid was then washed with dry pentane in the glovebox. The yellow solid was redissolved in 5 mL of dry air-free Et_2O within the glovebox and re-precipitated 2 – 3 times until a yellow microcrystalline solid was afforded. The final product yield was 74 % (131 mg, 0.25 mmol). ^{1}H NMR (CD_3NO_2, 400 MHz): δ 1.98 (s, 3H), 3.84 (s, 4H), 3.89 (s, 2H) 7.17-7.24 (m, 5H), 7.31 (br, 2H), 7.61 (br, 2H), 7.97 (br, 2H), 8.56 (br, 2H). Elemental Analysis ($C_{46}H_{20}BCuF_{20}N_4O$): Calculated; C, 51.01; H, 1.86; N, 5.17. Found; C, 50.92; H, 1.72; N, 4.79.

^{Bz}LCu^{I}-CO. In a 25 mL Schlenk flask equipped with a stirbar, a 5 – 10 mL CO saturated Et_2O solution was added to ^{Bz}LCu^{I} (144 mg, 0.16 mmol) via a cannula. While stirring, 20 mL of CO saturated dry pentane was added to the reaction solution and stirring continued for 15 minutes. The solution was then removed via cannula and dried under vacuum. The re-precipitation procedure was repeated 5 – 7 times until a white fluffy solid resulted. The final product yield was 82 % (131 mg, 0.25 mmol). ^{1}H NMR (CD_3NO_2, 400 MHz): δ 1.98 (s, 3H), 3.84 (s, 4H), 3.89 (s, 2H) 7.17-7.24 (m, 5H), 7.31 (br, 2H), 7.61 (br, 2H), 7.97 (br, 2H), 8.56 (br, 2H). Elemental Analysis ($C_{44}H_{19}BCuF_{20}N_3O$): Calculated; C, 49.86; H, 1.81; N, 3.96. Found; C, 49.60; H, 1.72; N, 4.28.

^{TBP}LCu^{I}-CO. In a 25 mL Schlenk flask equipped with a stirbar, a 5 – 10 mL CO saturated Et_2O solution was added to ^{Bz}LCu^{I} (144 mg, 0.16 mmol) via a cannula. While stirring, 20 mL of CO saturated dry pentane was added to the reaction solution and stirring continued for 15 minutes. The solution was then removed via cannula and dried under vacuum. The re-precipitation procedure was repeated 5 – 7 times until a white fluffy solid resulted. The final product yield was 87 % (131 mg, 0.25 mmol). ^{1}H NMR (CD_3NO_2, 400 MHz): δ 1.98 (s, 3H), 3.84 (s, 4H), 3.89 (s, 2H) 7.17-7.24 (m, 5H), 7.31 (br, 2H), 7.61 (br, 2H), 7.97 (br, 2H), 8.56 (br, 2H). Elemental Analysis ($C_{53}H_{30}BCuF_{20}N_4O$): Calculated; C, 53.35; H, 2.53; N, 4.70. Found; C, 52.81; H, 2.72; N, 4.57.

X-ray Crystallographic Studies. Crystalline materials for X-ray crystallographic analysis were prepared in a dry-box via dissolution of 5 mg of the copper(I) solvento species (^{TBP}LCu^{I}, ^{Bz}LCu^{I}, ^{Q}LCu^{I}) in dry deoxygenated Et_2O (~ 0.5 mL). The yellow solution was then transferred to a 9" (100 MHz) NMR tube and capped with a rubber septum. The samples were removed from the drybox and CO was sparged directly through the solution with a needle followed by layering of CO saturated pentane. Colorless crystals were afforded after 24 to 48 hours.

Crystals of each compound were placed in the N_2 cold stream (110 K) of an Oxford Xcaliber3 diffractometer at a distance of 50 mm from the CCD detector. The system was equipped with a graphite monochromator and an Enhance (Mo) X-ray Source (λ = 0.71073 Å) operated at 2 kW power (50 kV, 40 mA). Data frames were integrated with the Oxford Diffraction *CrysAlisRED* software package and the structures of ^{TBP}LCu^{I}-CO, ^{Bz}LCu^{I}-CO, and ^{Q}Cu^{I} were solved and refined using the Bruker *SHELXTL* (v6.1) software package. Analysis of the data showed negligible decay. Relevant crystallographic information is given in Table S1.

X-ray structural analysis was completed by two people: (1) Dr. Amy A. Narducci Sargeant, former staff crystallographer of the Chemistry Department at The Johns Hopkins University (JHU); her current employment is Northwestern University, Illinois; (2) Dr. Maxime A. Siegler, current JHU Chemistry Department staff crystallographer.

Table S1. Numerical crystal and refinement data for the X-ray crystal structures.

Complex	^{TBP}LCu^{I}-CO	^{Bz}LCu^{I}-CO	^{Q}LCu^{I}
formula (sum)	$C_{53}H_{30}BCuF_{20}N_4O$	$C_{44}H_{19}BCuF_{20}N_3O$	$C_{46}H_{20}BCuF_{20}N_4$
fw	1193.16	1059.97	1083.01
crystal system	Monoclinic	Monoclinic	Orthorhombic
space group	$P2_1/c$	$P2_1/c$	*Pbca*
a (Å)	16.5778(8)	14.3620(17)	20.1276(2)
b (Å)	16.6516(5)	17.989(3)	20.3135(2)
c (Å)	17.8893(7)	15.7391(17)	20.7405(2)
α (deg)	90	90	90
β (deg)	100.426(4)	94.130(9)	90
γ (deg)	90	90	90
V (Å^3)	4856.8(3)	4055.7(9)	8480.0(14)
Z	4	4	8
μ/mm^{-1} (Mo Kα)	0.573	0.673	0.646
reflections collected (total)	18 130	57 173	97 989
R_{int} (no. of equiv.	7842	9352	10479
observed reflections [I/s(I)	4791	6866	7762
Final R, Rw [I/σ(I) > 2]	0.0544, 0.1384	0.0309, 0.0797	0.0400, 0.1060

Infrared Spectroscopy. Room temperature infrared spectra were obtained using a Bruker Vector 33 FT-IR spectrophotometer. Instrument calibration was checked before each experiment by monitoring the characteristic vibrations of a polystyrene standard (IR-card). Solution samples of (~ 1 M) were prepared in 10 dram scintillation vials within an inert atmosphere dry-box by dissolution of the ligand-copper(I)-complexes (^{D}LCu^{I}) in THF solvent. The vials were stoppered with 14/20 red rubber septa, parafilmed, and removed from the drybox. The sample solutions were then saturated with CO and introduced through a 250 μL Hamilton syringe to a Spectralys Specac solution IR cell fit with potassium bromide (KBr) salt plates and capped. The neat solid CO stretching frequencies of the ligand-copper(I)-carbonyl compounds (^{D}LCu^{I}-CO) were obtained by slowing dripping the CO saturated THF sample solutions onto a round KBr crystal window (Aldrich). The samples were prepared under a CO atmosphere supplied by passing a positive flow of CO through a 100 mL funnel within the laboratory flow-hood.

Electrochemistry. Cyclic voltammetry studies were carried out using a Bioanalytical Systems BAS-100B electrochemistry analyzer. The cell was a standard three-electrode system with a platinum wire counter electrode, a glassy carbon working electrode, and a Ag/Ag^+ reference electrode. The measurements were performed at room temperature in CH_3CN solvent containing 100 mM tetrabutylammonium hexafluorophosphate (supporting electrolyte), 1 mM copper complex, and 1 mM ferrocene (internal standard). The air-sensitive samples were prepared under an inert atmosphere (drybox) in a 25 mL four-arm round bottom flask equipped with four 14/20 rubber septa. The flask was removed from the dry-box and each electrode was connected to the flask under positive argon pressure; electrodes were pierced through 14/20 rubber septa.

Gas Mixing. Carbon monoxide (CO; Air Gas East, grade 2.3) was treated by passing through an R & D Separations oxygen/moisture trap (Agilent Technologies OT3-4). Dioxygen (O_2; Air Gas East, grade 4.4) was dried by passing the gas through a short column of supported P_{4010} (Aquasorb, Mallinkrodt). Red rubber tubing (Fisher Scientific; inner diameter: 1/4 in.; thickness: 3/16 in.) was used to attach the gas cylinders fitted with appropriate regulators to two MKS Instruments Mass-Flo Controllers (MKS Type 1179A) regulated by an MKS Instruments Multi Channel Flow Ratio/Pressure Controller (MKS Type 647C). The gas mixtures were determined by the set flow rates of the two gases. For example, a 10% CO mixture would be made by mixing CO at a rate of 10 standard cubic centimeters per minute (sccm) with N_2 at 90 sccm for a total flow of 100 sccm. The CO concentration in solution was determined from the percent mixture and the literature values for CO saturation and adjusted for solvent contraction; for example in THF at 20°C, [CO] = 0.0109 M and $[O_2]$ = 0.010 M.

Low-temperature UV-visible Spectroscopy. Absorption spectra collected at −128°C were taken with a Cary 50 Bio spectrophotometer equipped with a fiber-optic coupler (Varian) and a fiber-optic

dip-probe (Hellma: 661.302-QX-UV-2mm-for-low-temperature). The −128°C cold bath consisted of a pentane and liquid nitrogen slurry confirmed by an Omega DPi32 thermocouple. The ligand-copper(I)-complexes (^{R}**LCu**^{I}) were prepared in MeTHF within custom reaction tubes (Chemglass) under an inert atmosphere (drybox). The reaction tubes were designed with a 24/40 joint that supplies an air-tight seal with the dip-probe through appropriately sized O-rings, a 14/20 side-arm for gas bubbling, and a Schlenk pressure/vacuum stopcock. Dioxygen was added by quickly bubbling the sample solution through a 24-inch (19-gauge) needle. A different UV-visible spectrophotometer and set-up was used to examine CO binding, see below.

Transient Absorbance Laser Flash Photolysis. Samples of ligand-copper(I)-carbonyl complexes (^{D}LCu^{I}-CO) were irradiated with λ_{ex} = 355 nm pulsed light (8 – 10 mJ/cm^2) using a Nd:YAG (Continuum Surelite III or a Big Sky Brilliant Blue) Q-switched laser on a previously described apparatus. The samples were probed at a right angle with a 150 W pulsed Xe lamp (Applied Photophysics) and protected with appropriate UV filters. Kinetic data was collected at monitored wavelengths (325 – 700 nm) from averages of 60 laser pulses. Variable low temperature studies (−85 to 20 °C) were performed using a Neslab ULT-95 Low-Temperature Bath/Circulator that delivers methanol through insulated tygon tubing to a custom copper coil made to fit a four-window UV-vis Dewar (H. S. Martin) filled with methanol. The Dewar was aligned with the pump/probe beams and the temperature was monitored by an Omega i-series thermocouple. Samples (1.5 mM) were prepared under an inert atmosphere (drybox) in 1 cm quartz cuvettes with four polished windows made custom by Quark glass. The cuvettes were equipped with a 14/20 joint and Schlenk stopcock atop a 20 – 25 cm column made to fit within the Dewar. Gas mixtures were added to sample solutions through direct bubbling through a 24-inch needle (19-gauge) for three

minutes. During data collection the gas flowed through the headspace of the sample cuvette and vented to an overhead laboratory exhaust system.

Determination of CO Binding Constants (K_{CO}) and Thermodynamic Parameters (ΔH^o; ΔS^o). UV-visible absorption spectra were obtained using a Hewlett-Packard 8453 diode array spectrophotometer equipped with a two-window quartz Dewar (H. S. Martin) filled with methanol. The temperature (–80 to 20 °C) of the Dewar was controlled by a setup similar to that described above utilizing a Neslab ULT-95 Low-Temperature Bath/Circulator that delivers methanol through a custom copper coil. Through spectrophotometric (UV-vis) titrations of CO/N_2 mixtures of precisely known concentrations, the equilibrium CO binding constant (K_{CO}) could be determined using eq 1. The gas mixtures were introduced into the cuvette using a 24 in. needle (19-gauge) and bubbling directly through the solution for ~30 seconds. The molar concentration of $[^{D}LCu^{I}\text{-}CO]^+$ was determined by application of eq 2 and calculated extinction coefficients (M^{-1} cm^{-1}). The molar concentration of $[^{D}LCu^{I}]^+$ could then be determined by subtracting $[^{D}LCu^{I}\text{-}CO]^+$ from the total concentration of the ligand-copper-complex species being studied, eq 3. Linear plots of [CO] vs. $[^{D}LCu^{I}\text{-}CO]^+/[^{D}LCu^{I}]^+$ afforded K_{CO}. Thermodynamic parameters (ΔH^o; ΔS^o) were obtained through Van't Hoff analyses (eq 4) by measuring K_{CO} as a function of temperature. Samples were equilibrated for a minimum of 3 minutes upon changing the temperature.

$$K_{CO} = \frac{[^{R}LCu^{I}\text{-}CO]^+}{[^{R}LCu^{I}]^+ [CO]} \qquad (1)$$

$$[^{R}LCu^{I}\text{-}CO]^+ = \frac{Abs_{\lambda max} - \varepsilon \times [^{R}LCu^{I}]^+_{TOT}}{\varepsilon_{[^{R}LCu^{I}\text{-}CO]^+} - \varepsilon_{[^{R}LCu^{I}]^+}} \qquad (2)$$

$$[^{R}LCu^{I}]^+ = [^{R}LCu^{I}]^+_{TOT} - [^{R}LCu^{I}\text{-}CO]^+ \qquad (3)$$

$$\ln (K_{CO}) = -\frac{\Delta H^o}{RT} + \frac{\Delta S^o}{R} \qquad (4)$$

Determination of the Bimolecular CO Binding Rate (k_{CO}), Dissociation Rate (k_{-CO}), and Activation Parameters ($\Delta H^{\ddagger}$; $\Delta S^{\ddagger}$). Photolysis (λ_{ex} = 355 nm) into the metal-to-ligand charge transfer (MLCT) band results in immediate formation of the ligand-copper(I)-solvento or naked (unsolvated) species ($^{D}LCu^{I}$) and free CO. The rate of CO rebinding (k_{obs}, s^{-1}) was then measured and analyzed using the first-order integrated rate law with ORIGIN 7.0 software. Gas concentrations (CO, N_2) were varied as described above in order to determine the bimolecular rate constants for CO binding, k_{CO} (M^{-1} s^{-1}), by applying eq 5. Activation parameters, $\Delta H^{\ddagger}$ (kJ mol^{-1}) and $\Delta S^{\ddagger}$ (J mol^{-1} K^{-1}), were determined through Eyring analyses (eq 6) of data collected from variable temperature work performed within the temperature range of 20 °C to –80 °C. The thermal CO dissociation rate, k_{-CO} (s^{-1}), was calculated through the use of eq 7; K_{CO} was determined through spectrophotometric CO titration experiments, see above.

$$k_{obs} = k_{CO}[CO] \tag{5}$$

$$\ln\left(\frac{k_{CO} \times h}{k_B \times T}\right) = -\frac{\Delta H^{\ddagger}}{RT} + \frac{\Delta S^{\ddagger}}{R} \tag{6}$$

$$K_{CO} = \frac{k_{CO}}{k_{-CO}} \tag{7}$$

Determination of the O_2 Binding Constant (K_{O2}), Thermodynamic Parameters (ΔH^{o}; ΔS^{o}), Bimolecular O_2 Binding Rate (k_{O2}), Dissociation Rate (k_{-O2}), and Activation Parameters ($\Delta H^{\ddagger}$; $\Delta S^{\ddagger}$). Photodissociation of CO from the ligand-copper(I)-carbonyl species ($^{Py}LCu^{I}$-CO, $^{Im}LCu^{I}$-CO, and $^{NMe_2}LCu^{I}$-CO) in the presence of O_2 resulted in fast O_2/CO competing reactions (k_{fast}, s^{-1}) with $^{Py}LCu^{I}$, $^{Im}LCu^{I}$, and $^{NMe_2}LCu^{I}$ that either regenerated the initial ligand-copper(I)-carbonyl species or formed a ligand-copper(II)-η^1-superoxo species ($^{D}LCu^{II}$-O_2^{-}). The bimolecular rate of O_2 binding,

k_{O2} (M^{-1} s^{-1}), was determined through analysis of the pseudo-first-order kinetic process (k_{fast}) in the presence of variable CO and O_2 concentrations. By applying eq 8, k_{O2} was obtained from the slope of the plot, $k_{fast} - k_{CO}[CO]$ vs. O_2; k_{CO} was determined in the absence of O_2 as described above. A second method for determining k_{O2} involved monitoring the slow equilibration (k_{slow}, s^{-1}) from the ligand-copper(II)-η^1-superoxo species ($^{D}LCu^{II}$-O_2^{-}) back to the initial ligand-copper(I)-carbonyl species. By applying eq 9 and plotting $1/k_{slow}$ vs. $[O_2]/[CO]$, the equilibrium constant for O_2 binding (K_{O2}) and the O_2 dissociation rate constants (k_{-O2}) are directly determined. Application of eq 10 readily leads to k_{O2}. Activation parameters, $\Delta H^{\ddagger}$ (kJ mol^{-1}) and $\Delta S^{\ddagger}$ (J mol^{-1} K^{-1}), associated with k_{O2} and k_{-O2} were determined through Eyring analyses (eq 11) of k_{slow} collected within the temperature range −55°C to −85°C under precise CO/O_2 gas mixtures. Thermodynamic parameters, ΔH^{o} (kJ mol^{-1}) and ΔS^{o} (J mol^{-1} K^{-1}), were determined through eq 12.

$$k_{fast} = k_{CO}[CO] + k_{O2}[O_2] \tag{8}$$

$$\frac{1}{k_{slow}} = \frac{K_{O2}[O_2]}{k_{CO}[CO]} + \frac{1}{k_{-O2}} \tag{9}$$

$$K_{O2} = \frac{k_{O2}}{k_{-O2}} \tag{10}$$

$$\ln\left(\frac{k_{O2} \times h}{k_B \times T}\right) = -\frac{\Delta H^{\ddagger}}{RT} + \frac{\Delta S^{\ddagger}}{R} \tag{11}$$

$$\ln(K_{O2}) = -\frac{\Delta H^{o}}{RT} + \frac{\Delta S^{o}}{R} \tag{12}$$

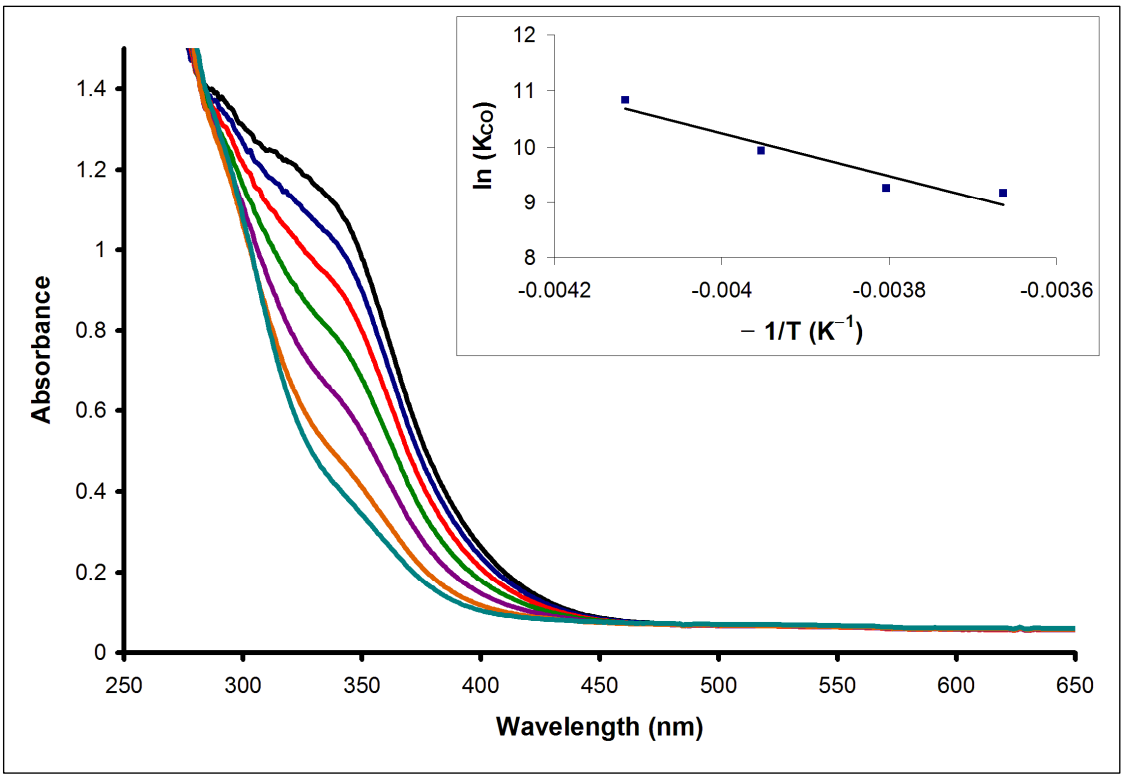

Figure S01. Spectrophotometric titration of CO to ^{Im}**LCu**^{I} in THF at room temperature. The inset is a Van't Hoff plot (R = 0.96) of the variable temperature K_{CO} data collected from –40 °C to 20 °C.

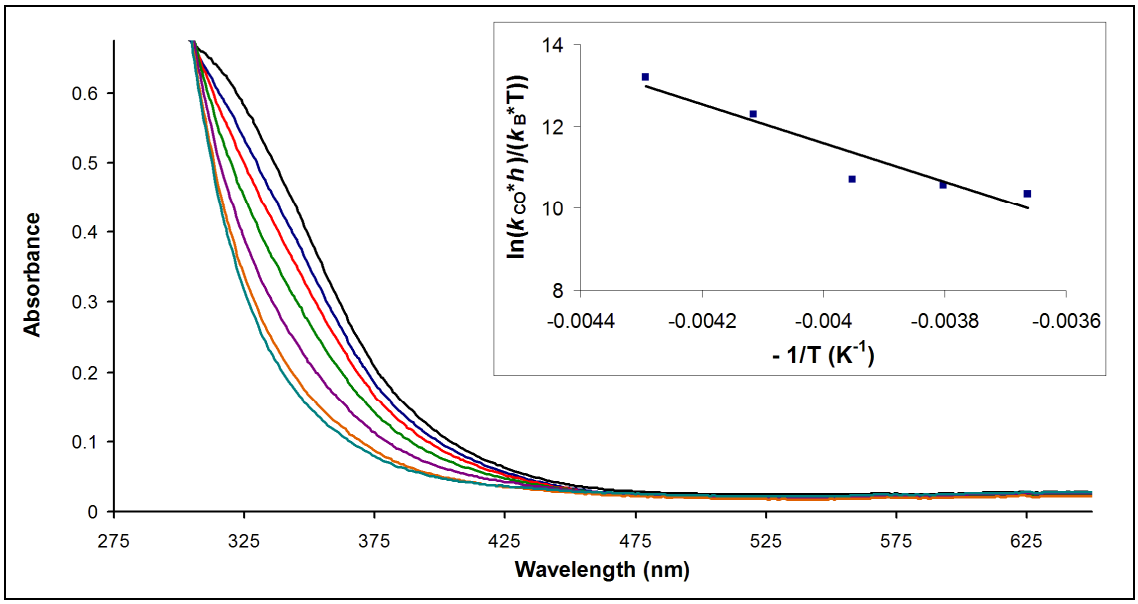

Figure S02. Spectrophotometric titration of CO to ^{NMe_2}**LCu**^{I} in THF at room temperature. The inset is a Van't Hoff plot (R = 0.95) of the variable temperature K_{CO} data collected from –40 °C to 20 °C.

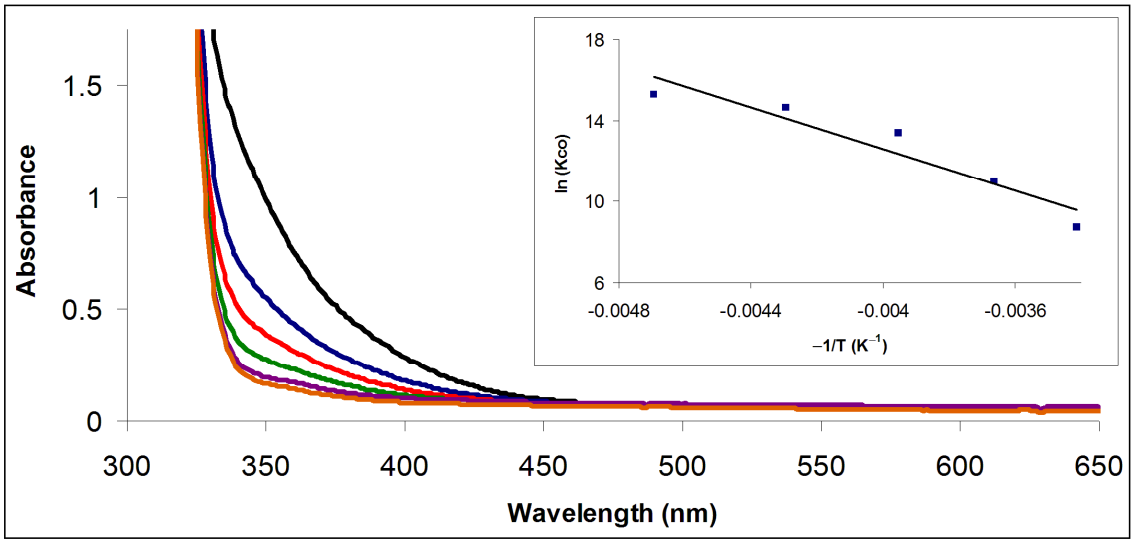

Figure S03. Spectrophotometric titration of CO to ^{Q}**LCu**^{I} in THF at room temperature. The inset is a Van't Hoff plot (R = 0.96) of the variable temperature K_{CO} data collected from –40 °C to 20 °C.

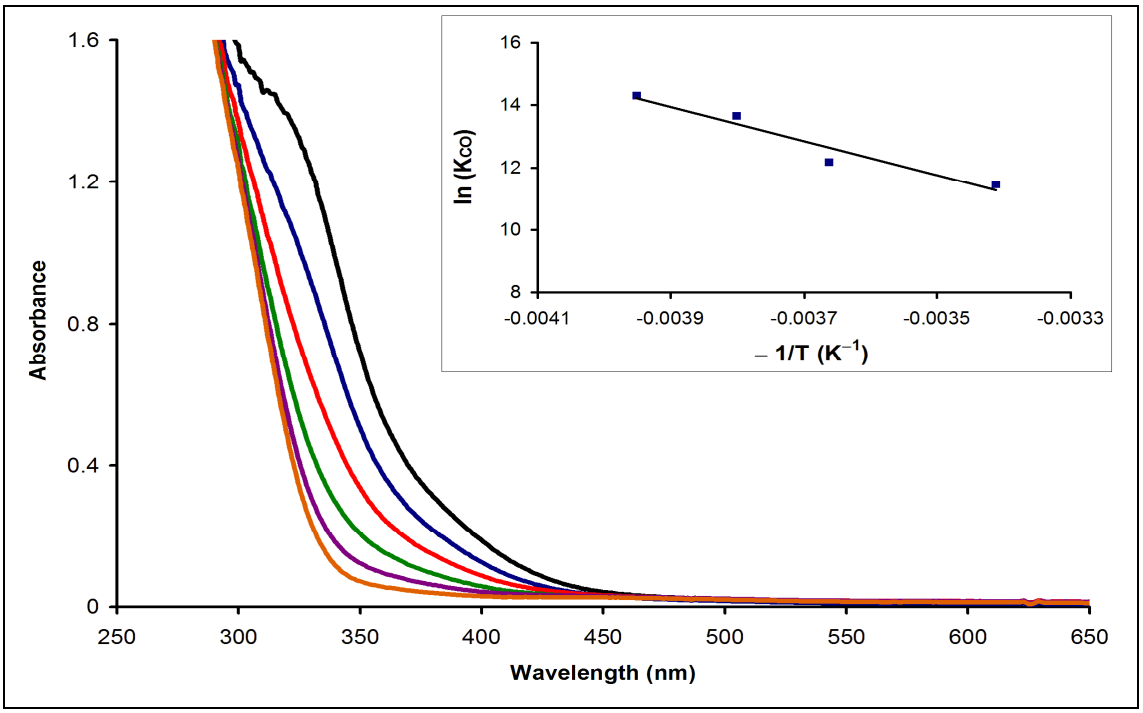

Figure S04. Spectrophotometric titration of CO to ^{Bz}**LCu**^{I} in THF at room temperature. The inset is a Van't Hoff plot (R = 0.97) of the variable temperature K_{CO} data collected from –30 °C to 20 °C.

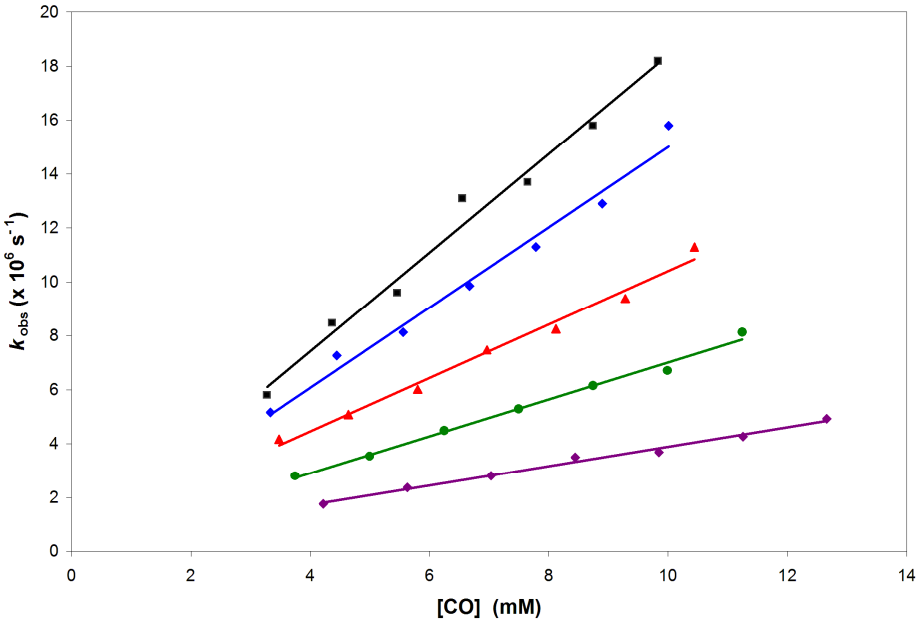

Figure S05. Temperature dependence and [CO] dependence of pseudo-first order CO recombination to ^{Im}**LCu**^{I} in THF (k_{obs} vs. [CO]) obtained by transient absorbance laser flash photolysis experiments: black squares (R = 0.98), 273 K; blue diamonds (R = 0.98), 253 K; red triangles (R = 0.99), 233 K; green circles (R = 0.99), 213 K; purple diamonds (R = 0.99), 193 K. The slope of each line corresponds directly to the bimolecular rate constant of CO recombination, k_{CO} (M^{-1} s^{-1}).

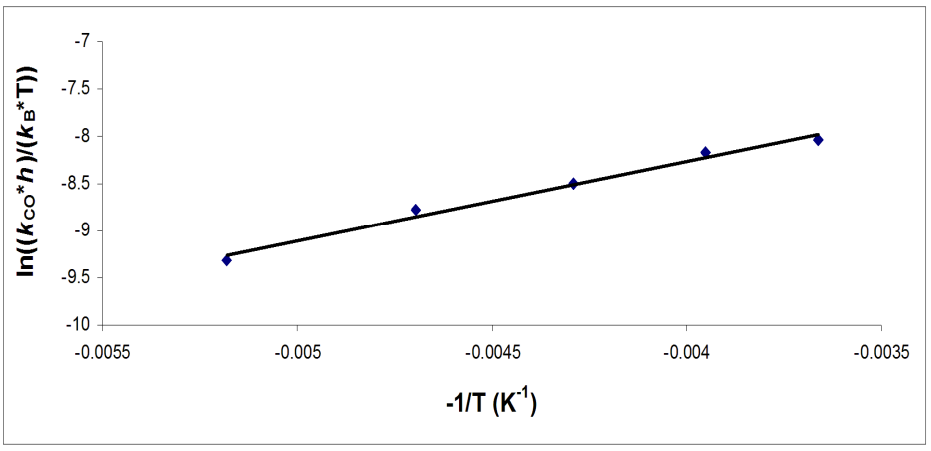

Figure S06. Eyring analysis (R = 0.99) of bimolecular CO recombination to ^{Im}**LCu**^{I} in THF solvent at various temperatures, 193 – 273 K. The slope affords the activation enthalpy $\Delta H^{\ddagger}$ = 7.03 kJ mol^{-1} and the intercept affords the activation entropy $\Delta S^{\ddagger}$ = –40.5 J mol^{-1} K^{-1}.

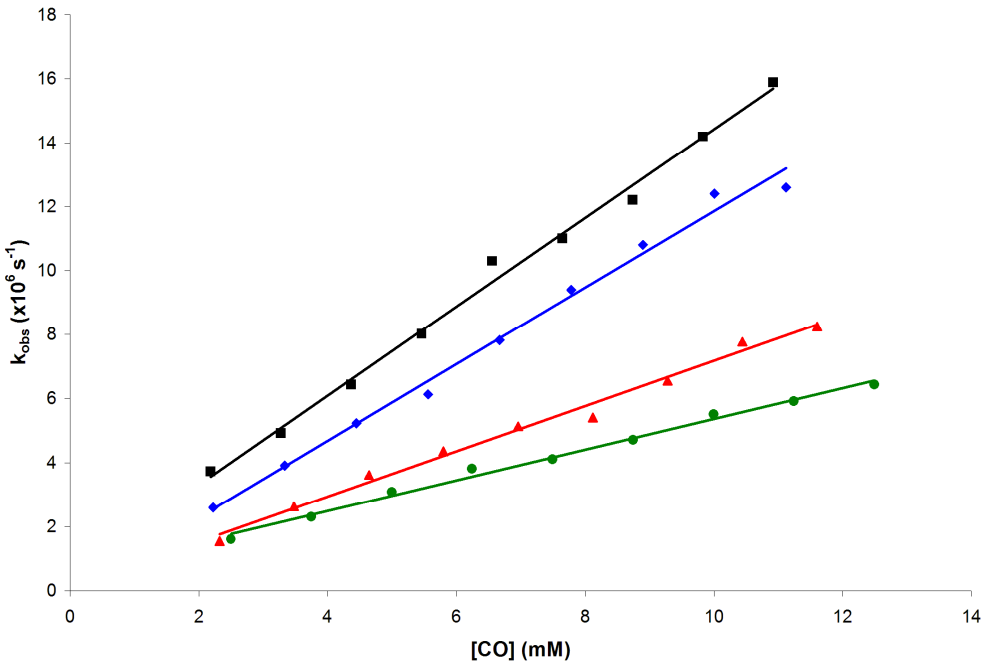

Figure S07. Temperature dependence and [CO] dependence of pseudo-first order CO recombination to ^{NMe_2}**LCu**^{I} in THF (k_{obs} vs. [CO]) obtained by transient absorbance laser flash photolysis experiments: black squares (R = 0.99), 273 K; blue diamonds (R = 0.99), 253 K; red triangles (R = 0.99), 233 K; green circles (R = 0.99), 213 K. The slope of each line corresponds directly to the bimolecular rate constant of CO recombination, k_{CO} (M^{-1} s^{-1}).

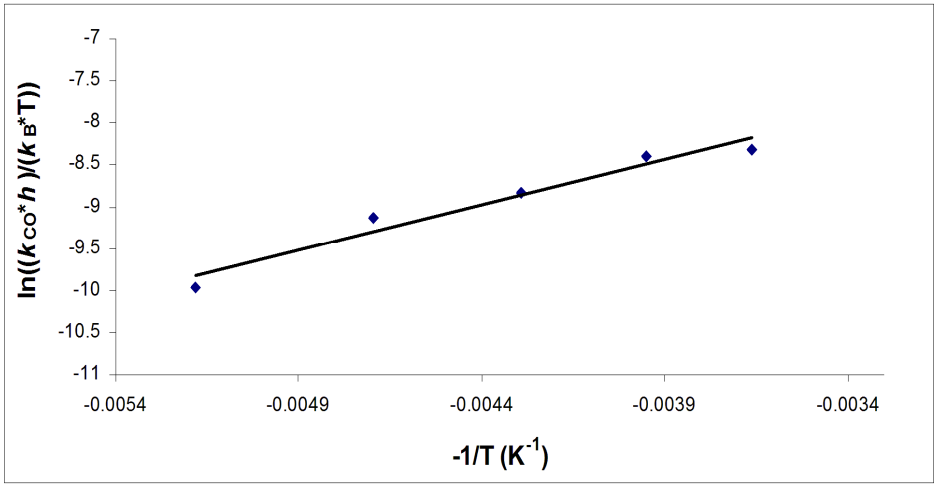

Figure S08. Eyring analysis (R = 0.98) of bimolecular CO recombination to ^{NMe_2}**LCu**^{I} in THF solvent at various temperatures, 193 – 273 K. The slope affords the activation enthalpy $\Delta H^{\ddagger}$ = 9.07 kJ mol^{-1} and the intercept affords the activation entropy $\Delta S^{\ddagger}$ = –34.7 J mol^{-1} K^{-1}.

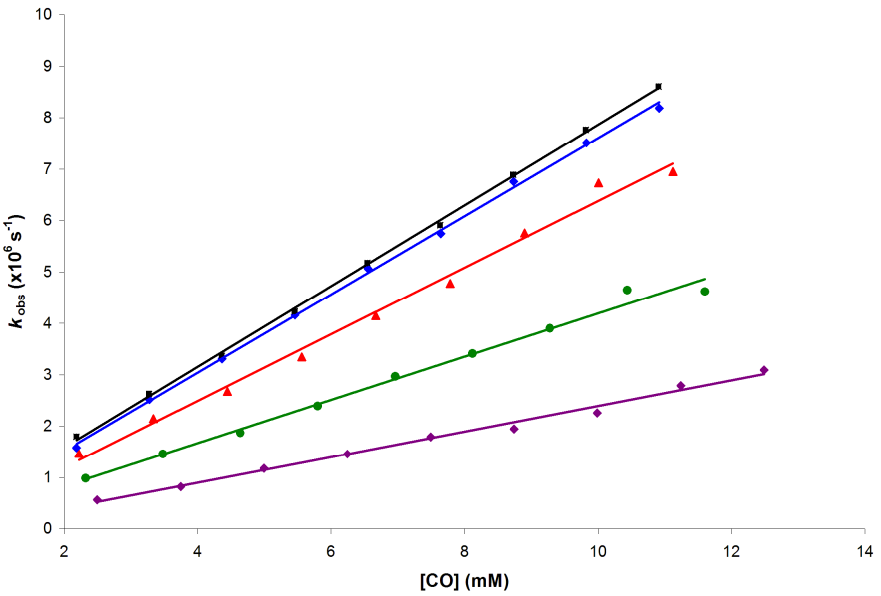

Figure S09. Temperature dependence and [CO] dependence of pseudo-first order CO recombination to ^{Q}**LCu**^{I} in THF (k_{obs} vs. [CO]) obtained by transient absorbance laser flash photolysis experiments: black squares (R = 0.99), 293 K; blue diamonds (R = 0.99), 273 K; red triangles (R = 0.99), 253 K; green circles (R = 0.99), 233 K; purple diamonds (R = 0.99), 213 K. The slope of each line corresponds directly to the bimolecular rate constant of CO recombination, k_{CO} (M^{-1} s^{-1}).

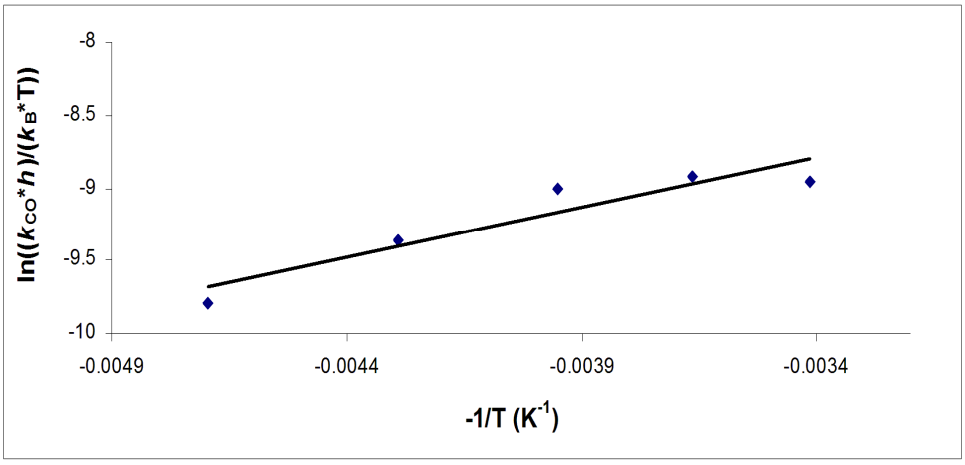

Figure S10. Eyring analysis (R = 0.93) of bimolecular CO recombination to ^{Q}**LCu**^{I} in THF solvent at various temperatures, 213 – 293 K. The slope affords the activation enthalpy $\Delta H^{\ddagger}$ = 5.66 kJ mol^{-1} and the intercept affords the activation entropy $\Delta S^{\ddagger}$ = –53.9 J mol^{-1} K^{-1}.

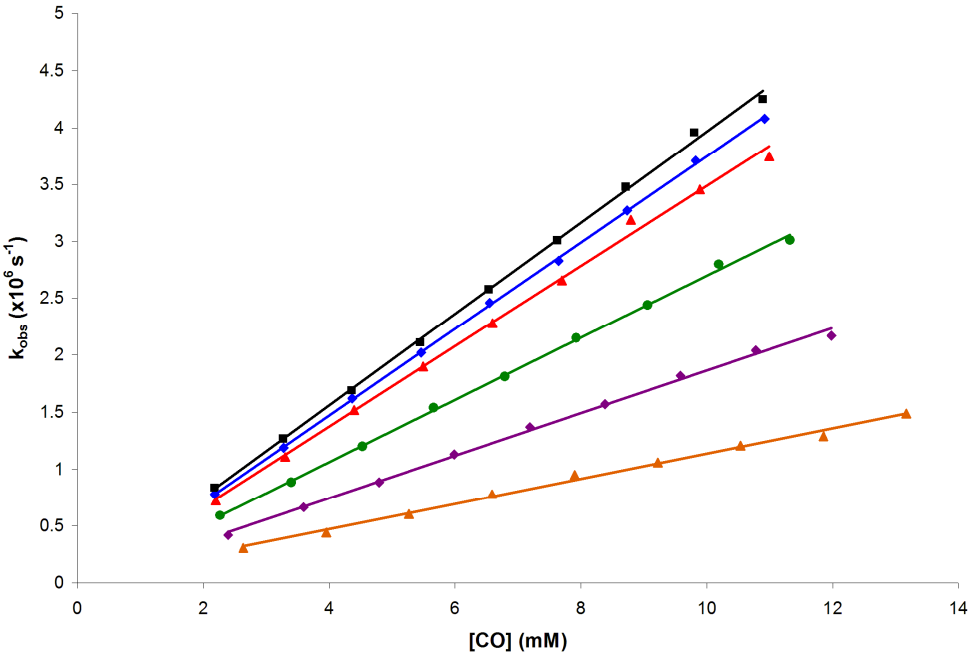

Figure S11. Temperature dependence and [CO] dependence of pseudo-first order CO recombination to ^{TBP}**LCu**^{I} in THF (k_{obs} vs. [CO]) obtained by transient absorbance laser flash photolysis experiments: black squares (R = 0.99), 283 K; blue diamonds (R = 0.99), 273 K; red triangles (R = 0.99), 263 K; green circles (R = 0.99), 243 K; purple diamonds (R = 0.99), 223 K; orange triangles (R = 0.99), 203 K. The slope of each line corresponds directly to the bimolecular rate constant of CO recombination, k_{CO} (M^{-1} s^{-1}).

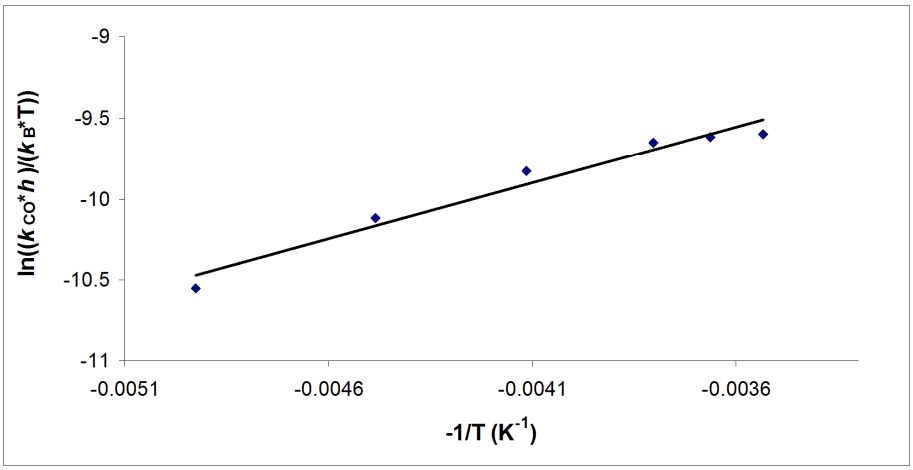

Figure S12. Eyring analysis (R = 0.98) of bimolecular CO recombination to ^{TBP}**LCu**^{I} in THF solvent at various temperatures, 283 – 203 K. The slope affords the activation enthalpy $\Delta H^{\ddagger}$ = 5.76 kJ mol^{-1} and the intercept affords the activation entropy $\Delta S^{\ddagger}$ = –58.7 J mol^{-1} K^{-1}.

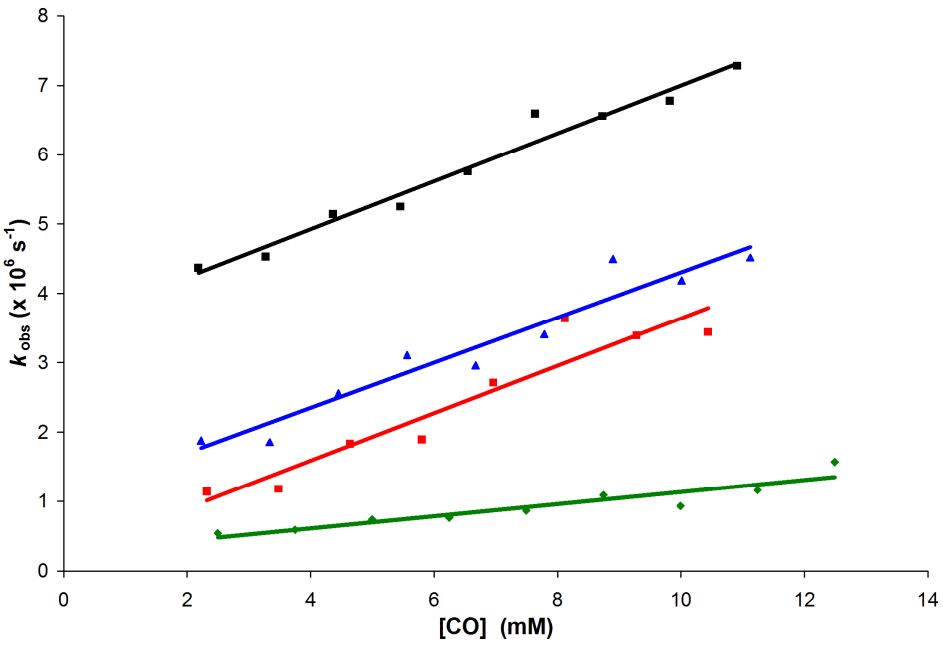

Figure S13. Temperature dependence and [CO] dependence of pseudo-first order CO recombination to ^{Bz}**LCu**^{I} in THF (k_{obs} vs. [CO]) obtained by transient absorbance laser flash photolysis experiments: black squares (R = 0.98), 293 K; blue diamonds (R = 0.96), 253 K; red squares (R = 0.94), 233 K; green circles (R = 0.99), 213 K. The slope of each line corresponds directly to the bimolecular rate constant of CO recombination, k_{CO} (M^{-1} s^{-1}).

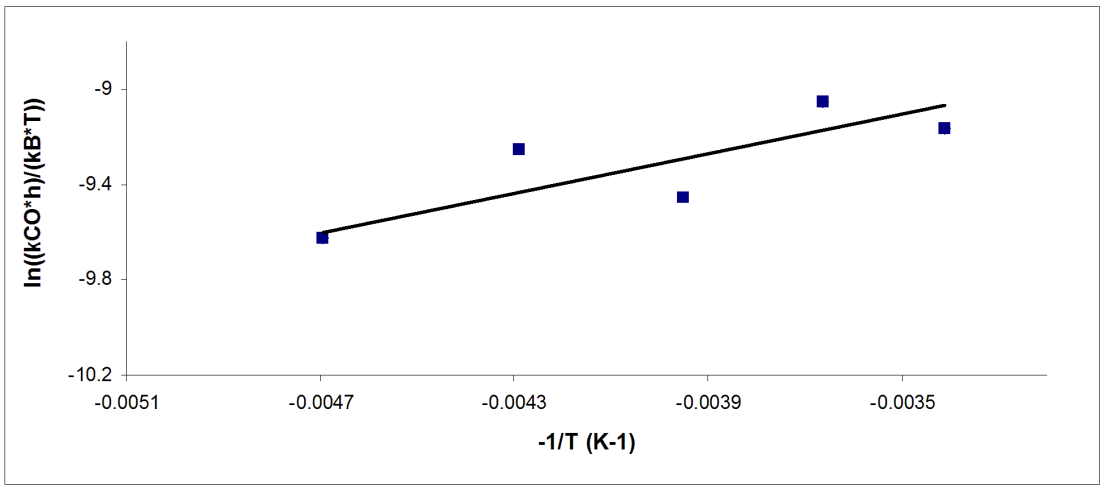

Figure S14. Eyring analysis (R = 0.93) of bimolecular CO recombination to ^{Bz}**LCu**^{I} in THF solvent. The slope affords the activation enthalpy $\Delta H^{\ddagger}$ = 0.7 kJ mol^{-1} and the intercept affords the activation entropy $\Delta S^{\ddagger}$ = –76 J mol^{-1} K^{-1}.

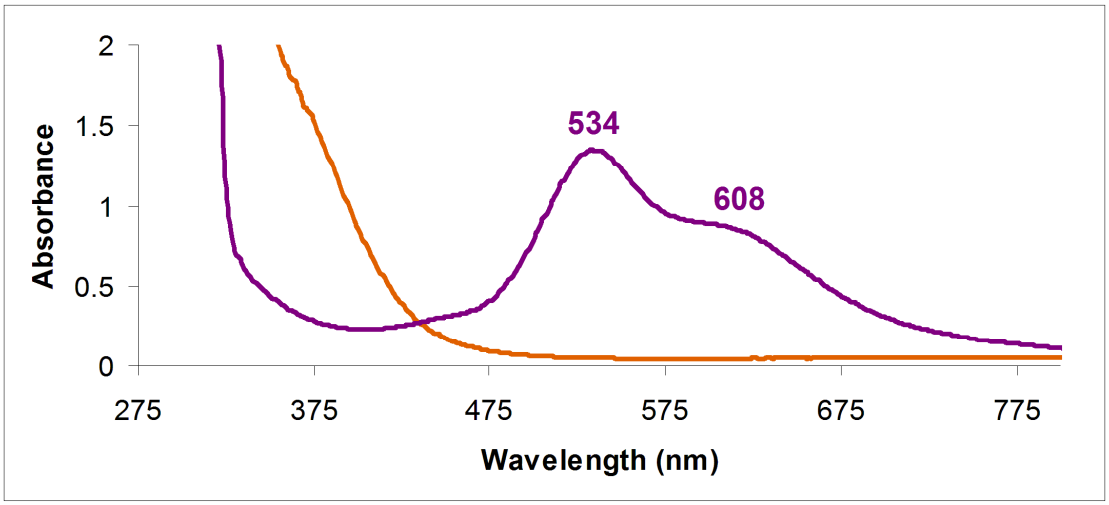

Figure S15. UV-visible spectra in MeTHF at −128 °C illustrating the formation of the dicopper(II)-μ-1,2-peroxo complex $\{^{Q}LCu^{II}\}_2(O_2^{2-})]^{2+}$ following the addition of O_2 to $^{Q}LCu^{I}$.

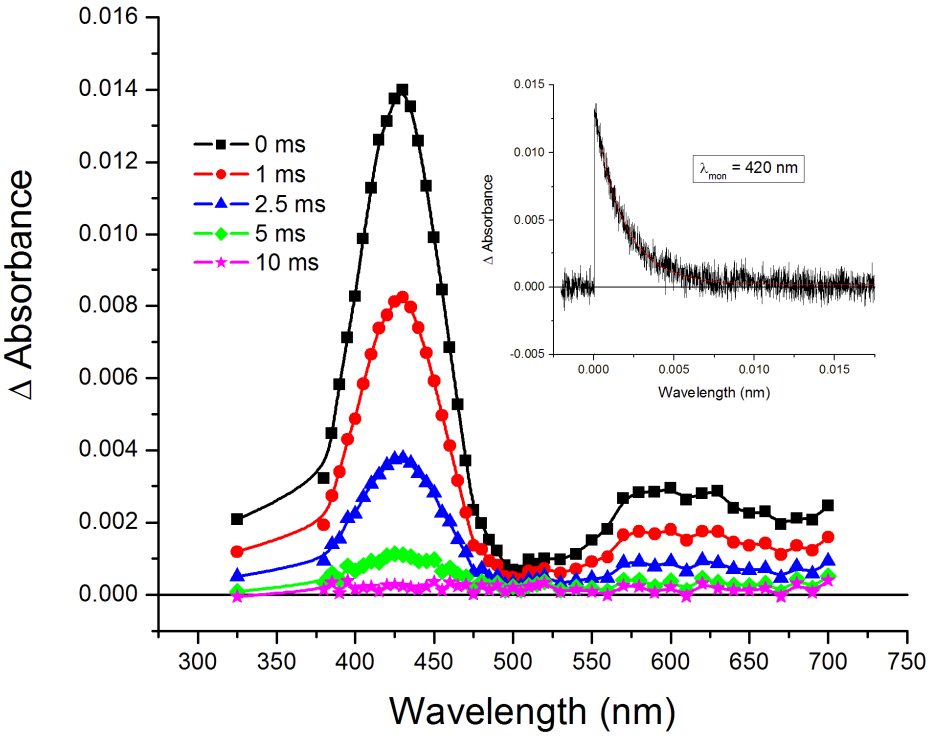

Figure S16: Transient absorption difference spectra illustrating the slow equilibration (k_{slow}) from $^{Im}LCu^{II}\text{-}O_2^{-}$ to $^{Im}LCu^{I}\text{-}CO$ in THF at −80 °C at various delay times: 0 ms (black squares); 1 ms (red circles); 2.5 ms (blue triangles); 5 ms (green diamonds); 10 ms (pink stars). The inset is a kinetic trace with a pseudo-1st order kinetic fit collected at λ_{mon} = 420 nm.

Table S2. Bimolecular rate constants k_{O2} determined from k_{slow} for $^{Im}LCu^{II}\text{-}O_2^-$ and $^{NMe_2}LCu^{II}\text{-}O_2^-$ at various temperatures.

TEMP	$^{Im}LCu^{II}\text{-}O_2^-$ (M^{-1} s^{-1})	$^{NMe_2}LCu^{II}\text{-}O_2^-$ (M^{-1} s^{-1})
– 60 °C	(7.3 ± 0.01) x 10^8	(6.0 ± 0.05) x 10^8
– 65 °C	(4.8 ± 0.06) x 10^8	(3.9 ± 0.02) x 10^8
– 70 °C	(3.2 ± 0.01) x 10^8	(3.0 ± 0.04) x 10^8
– 75 °C	(1.9 ± 0.04) x 10^8	(2.1 ± 0.09) x 10^8
– 80 °C	(1.8 ± 0.03) x 10^8	(6.9 ± 0.02) x 10^7

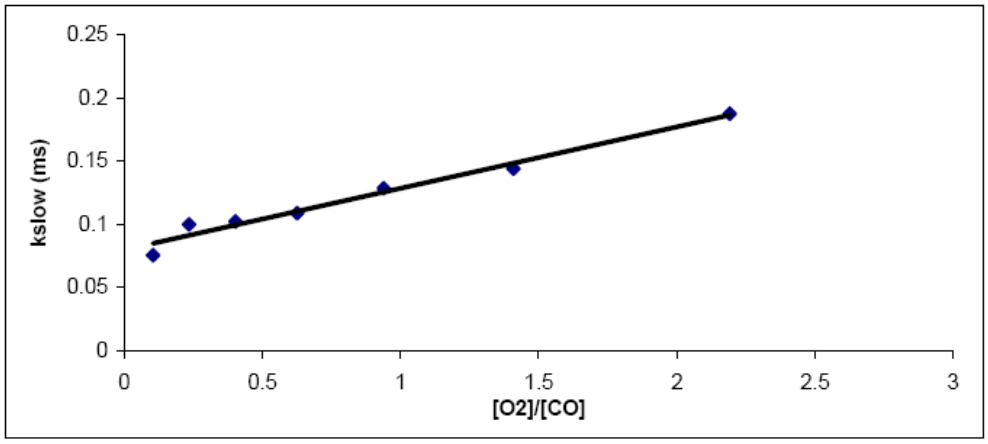

Figure S17. Plot (R = 0.98) of $1/k_{slow}$ vs. $[O_2]/[CO]$ at –67 °C for determination of K_{O2} and k_{-O2} for $^{Im}LCu^{II}\text{-}O_2^-$, which readily gives to k_{O2}.

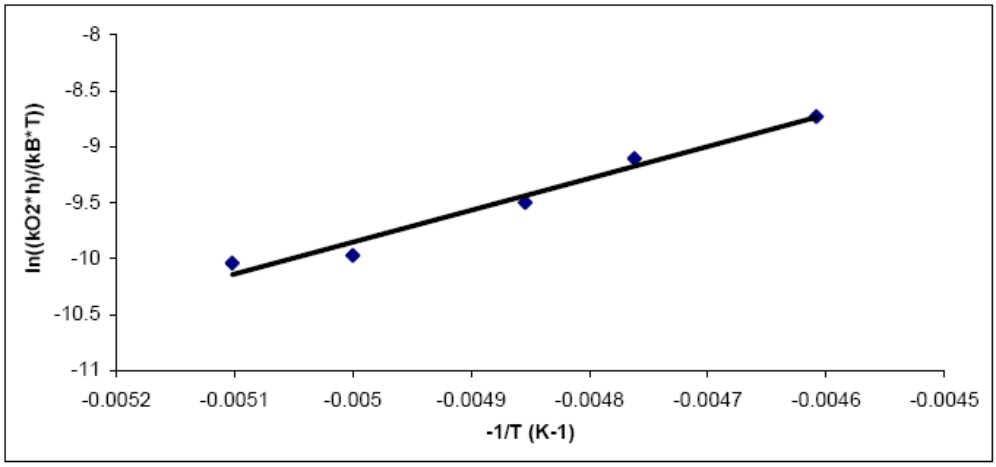

Figure S18. Eyring analysis plot (R = 0.98) for formation of $^{Im}LCu^{II}\text{-}O_2^-$ of the k_{O2} data collected at variable temperature (–80 °C to –60 °C).

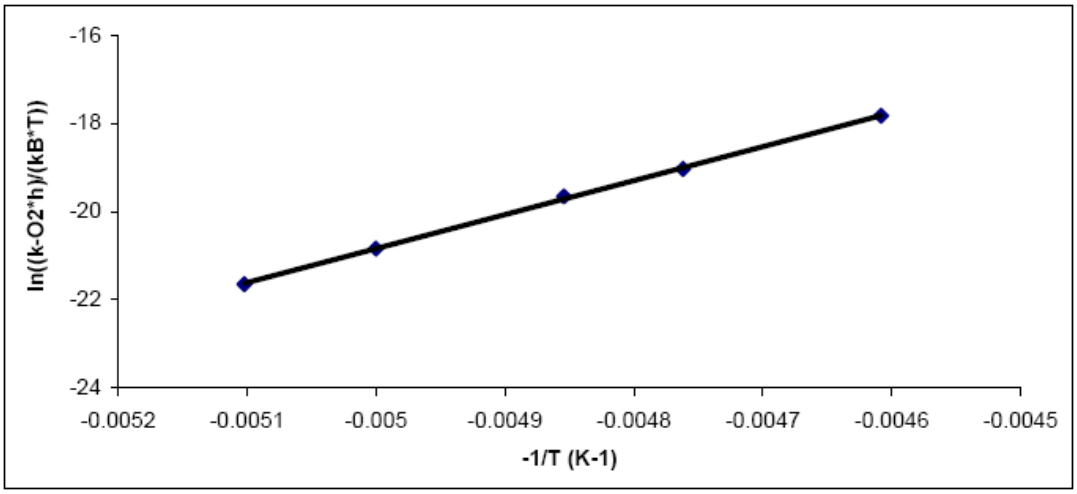

Figure S19. Eyring analysis plot (R = 0.99) for formation of ^{Im}**LCu^{II}-O$_2^-$** of the k_{-O2} data collected at variable temperature (–80 °C to –60 °C).

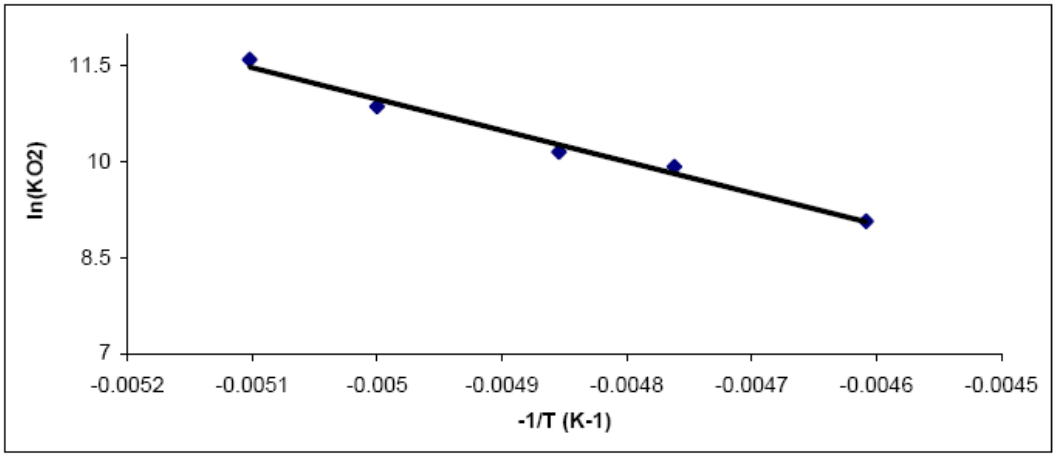

Figure S20. Van't Hoff plot (R = 0.99) of variable temperature K_{O2} data for ^{Im}**LCu^{II}-O$_2^-$** collected from –80 °C to –60 °C.

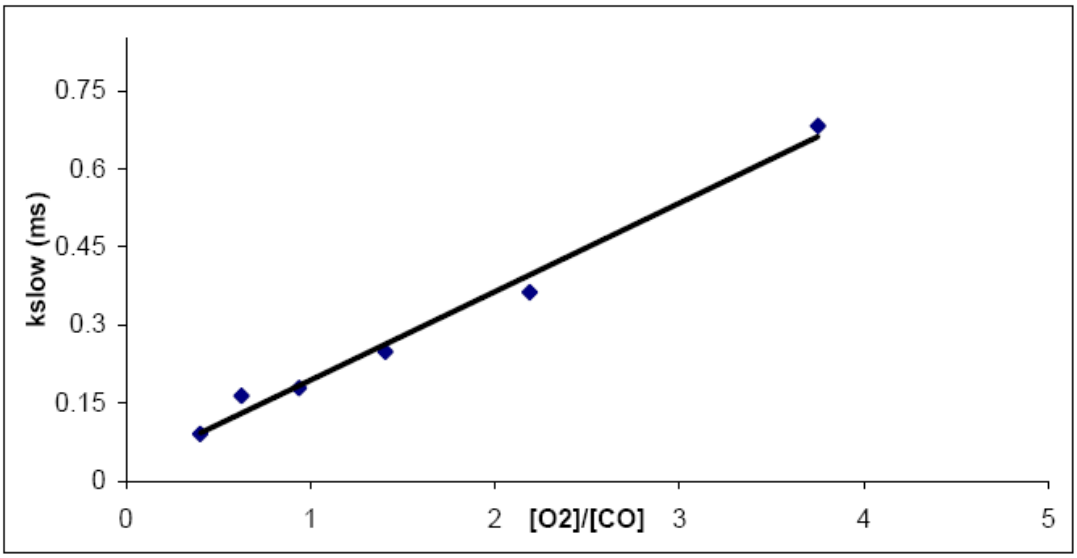

Figure S21. Plot (R = 0.99) of $1/k_{slow}$ vs. $[O_2]/[CO]$ at –65 °C for determination of K_{O2} and k_{-O2} for ^{NMe_2}**LCu^{II}-O$_2^-$**, which readily gives to k_{O2}.

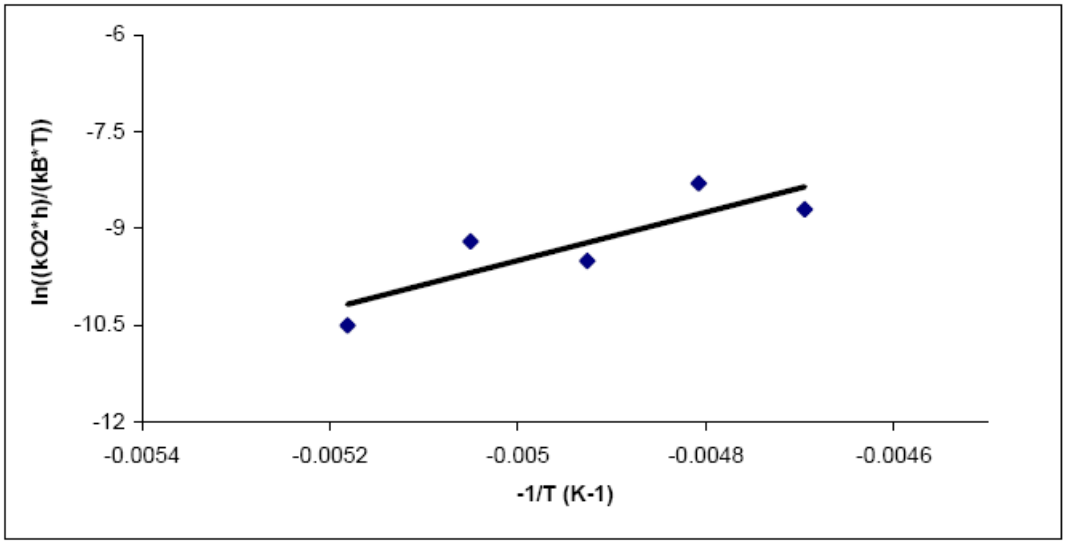

Figure S22. Eyring analysis plot (R = 0.85) for formation of ^{NMe_2}**LCu^{II}-O$_2^-$** of the k_{O2} data collected at variable temperature (–80 °C to –60 °C).

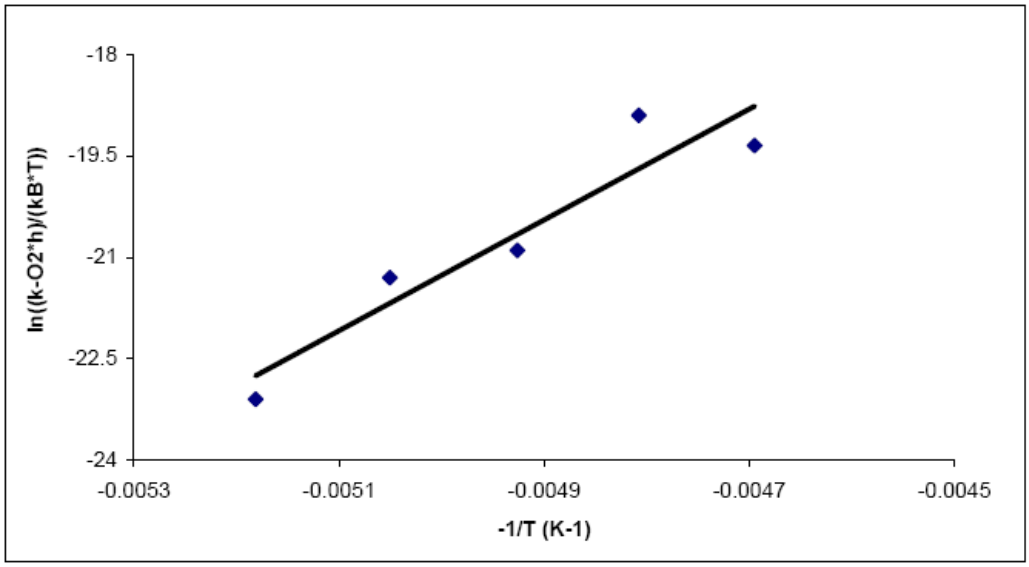

Figure S23. Eyring analysis plot (R = 0.94) for formation of ^{NMe_2}**LCu^{II}-O$_2^{-}$** of the k_{-O2} data collected at variable temperature (–80 °C to –60 °C).

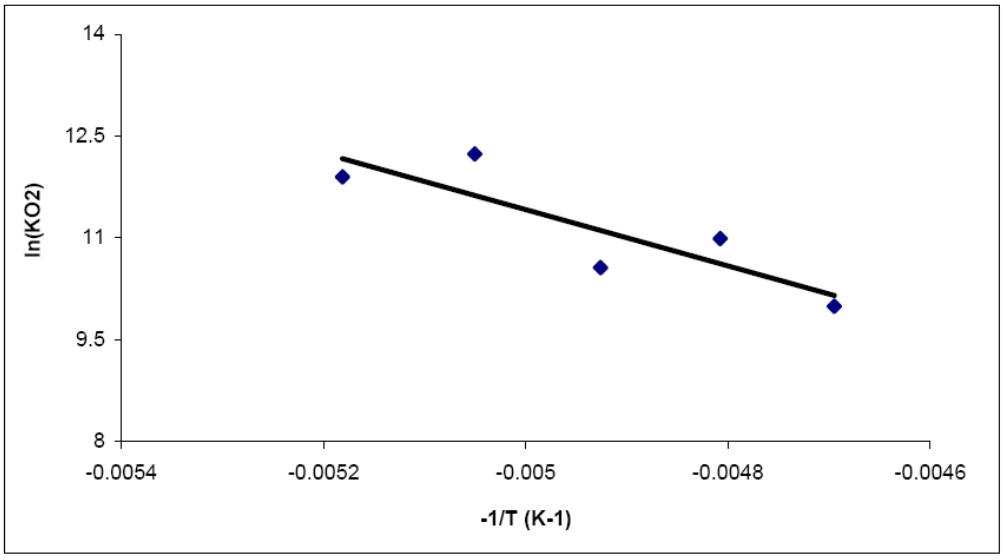

Figure S24. Van't Hoff plot (R = 0.86) of variable temperature K_{O2} data for ^{NMe_2}**LCu^{II}-O$_2^{-}$** collected from –80 °C to –60 °C.